microbial biotechnology

Open Access

High-throughput dilution-based growth method enables time-resolved exo-metabolomics of *Pseudomonas putida* and *Pseudomonas aeruginosa*

Bjarke H. Pedersen,[1] Nicolás Gurdo,[1] Helle Krogh Johansen,[1,2,3] Søren Molin,[1] Pablo I. Nikel[1] and Ruggero La Rosa[1]

[1]*The Novo Nordisk Foundation Center for Biosustainability, Technical University of Denmark, Kgs. Lyngby, 2800, Denmark.*

[2]*Department of Clinical Microbiology, 9301, Rigshospitalet, Copenhagen, 2100, Denmark.*

[3]*Department of Clinical Medicine, Faculty of Health and Medical Sciences, University of Copenhagen, Copenhagen, 2200, Denmark.*

High-throughput dilution-based growth method enables time-resolved exo-metabolomics of *Pseudomonas putida* and *Pseudomonas aeruginosa*. Bjarke H. Pedersen, Nicolás Gurdo, Helle Krogh Johansen, Søren Molin, Pablo I. Nikel and Ruggero La Rosa. Microbial Biotechnology (2021) 14(5), 2214–2226. doi:10.1111/1751-7915.13905

Summary

Understanding metabolism is fundamental to access and harness bacterial physiology. In most bacteria, nutrient utilization is hierarchically optimized according to their energetic potential and their availability in the environment to maximise growth rates. Low-throughput methods have been largely used to characterize bacterial metabolic profiles. However, in-depth analysis of large collections of strains across several conditions is challenging since high-throughput approaches are still limited – especially for non-traditional hosts. Here, we developed a high-throughput dilution-resolved cultivation method for metabolic footprinting of *Pseudomonas putida* and *Pseudomonas aeruginosa*. This method was benchmarked against a conventional low-throughput time-resolved cultivation approach using either a synthetic culture medium (where a single carbon source is present) for *P. putida* or a complex nutrient mixture for *P. aeruginosa*. Dynamic metabolic footprinting, either by sugar quantification or by targeted exo-metabolomic analyses, revealed overlaps between the bacterial metabolic profiles irrespective of the cultivation strategy, suggesting a certain level of robustness and flexibility of the high-throughput dilution-resolved method. Cultivation of *P. putida* in microtiter plates imposed a metabolic constraint, dependent on oxygen availability, which altered the pattern of secreted metabolites at the level of sugar oxidation. Deep-well plates, however, constituted an optimal cultivation set-up yielding consistent and comparable metabolic profiles across conditions and strains. Altogether, the results illustrate the usefulness of this technological advance for high-throughput analyses of bacterial metabolism for both biotechnological applications and automation purposes.

Introduction

Bacterial metabolism comprises sets of biochemical reactions that are tightly regulated spatio-temporally. This complex network of reactions interacts dynamically with the external environment. Thus, changes in the surrounding conditions (e.g. nutrient availability) are propagated to the intracellular metabolites' fluxes to optimize cellular physiology (Chubukov *et al*., 2014). Microbial growth is, indeed, influenced by the availability of the nutritional resources, which is often a matrix of several different components (Sezonov *et al*., 2007; Molina *et al*., 2019b).

Due to the tight relationship between exo- and endo-metabolism, variations in exo-metabolites provide important information on the intracellular metabolic status of the cell (Mapelli *et al*., 2008). Metabolic footprinting analysis allows quantification of metabolite depletion and/or synthesis as function of the cellular growth, which can be further used as constraints for genome-scale metabolic models for the computation of intracellular metabolite distribution and fluxes (Mapelli *et al*., 2008; O'Brien *et al*., 2015). For this reason, exo-metabolomic analyses have been extensively used for a variety of both biotechnological applications and for basic research, such as the functional characterization of uncharacterized genes, selection of evolved strains, identification of relevant bacterial mutants, and description of metabolic pathways in several bacterial species (Kaderbhai *et al*., 2003; Howell *et al*., 2006; Henriques *et al*., 2007; Paczia *et al*., 2012; Deutschbauer *et al*., 2014).

In Pseudomonads, metabolic footprinting has been primarily used to characterize regulatory processes such

Received 10 May, 2021; revised 5 July, 2021; accepted 18 July, 2021.

For correspondence. E-mail rugros@biosustain.dtu.dk; Tel: (+45) 9351 1647.

Microbial Biotechnology (2021) **14**(5), 2214–2226
doi:10.1111/1751-7915.13905

as Carbon Catabolite Repression (CCR), proteome composition changes as function of cellular growth, and to identify links between metabolism and infection (Behrends *et al*., 2009, 2013; La Rosa *et al*., 2016, 2018; Yung *et al*., 2019; Arce-Rodríguez *et al*., 2021; McGill *et al*., 2021). Pseudomonads constitute a large group of bacterial species of high interest, both from biotechnological and clinical points of view (Weimer *et al*., 2020; Rossi *et al*., 2021). *Pseudomonas putida* is a valuable chassis organism due to its broad metabolic capability, high tolerance to harsh conditions (oxidative stress and toxic compounds), fast growth in multiple laboratory conditions, and for the availability of a vast spectrum of genetic tools to manipulate its genome (Nikel *et al*., 2014). *P. aeruginosa* is a ubiquitous human opportunistic pathogen present in different natural environments, and associated with pulmonary infections in cystic fibrosis (CF) patients, burn wounds, urinary tract infections and hospital-acquired infections (Crone *et al*., 2020). In both *P. putida* and *P. aeruginosa*, the utilization of essential metabolites in simple or complex mixtures is a dynamic process orchestrated by several regulators (Behrends *et al*., 2013; Nikel *et al*., 2014, 2015; La Rosa *et al*., 2016, 2019; Molina *et al*., 2019a, 2019b; Dolan *et al*., 2020). Glucose assimilation occurs through oxidization in the periplasm, first to gluconate (GA) and then to 2-ketogluconate (2-KGA), which are subsequently phosphorylated to glucose-6-phosphate (G6P), 6-phosphogluconate (6PG) or 2-keto-6-phosphogluconate (2KG) to enter the cytoplasm (del Castillo *et al*., 2007; Nikel *et al*., 2015, 2021). In rich complex media, the CCR complex Crc/Hfq represses the assimilation of less preferred carbon sources, such as glucose or branched-chain amino acids, favouring the assimilation of other more energetically preferred nutrients, such as glutamine, asparagine, aspartate, alanine and glutamate (Rojo, 2010; La Rosa *et al*., 2016).

Conventionally, to study exo-metabolite dynamics, cell cultures are established in Erlenmeyer flasks and supernatant samples are continuously collected from the same culture. This classical approach is called the 'time-resolved' method (Fig. 1). Importantly, the higher the number of data points to collect, the higher the volume of cell culture needed. This reduces the effect of sampling on the physiology of the cell as a consequence of the shift in the culture volume/conditions over time (Behrends *et al*., 2014). Although the conventional time-resolved method provides detailed analyses of metabolite uptake/secretion profiles, it is clearly a low-throughput method when many samples are needed, and many strains are analysed. High-throughput methodologies such as 'dilution-resolved' synchronized cell culture can, theoretically, be applied to multiple conditions and several strains on 96-well plates, substantially increasing the throughput (Govantes, 2018). This method, first described by van Ditmarsch and colleagues (van Ditmarsch and Xavier, 2011; López-Sánchez *et al*., 2013), takes advantage of the relationship between the lag phase of growth and the cell density, and offers a great potential for many biotechnological applications. In practice, serial dilutions of bacterial cell cultures are established to generate shifts in the growth curves reflecting the differences in the initial biomass concentration. After incubation, all samples are simultaneously harvested, and each end-point sample from the different dilutions is synchronized to reconstruct the time-dependent trajectory of a conventional time-resolved growth curve (Fig. 1). A detailed description of the method and a detailed protocol are available in REF (Govantes, 2018). However, even though this method appears to be very promising, only a limited number of examples are available in literature (van Ditmarsch and Xavier, 2011; López-Sánchez *et al*., 2013, 2016; Jiménez-Fernández *et al*., 2015, 2016; Govantes, 2018). Whether the dilution-resolved method for high-throughput applications secures flexibility in terms of cultivation set-ups which entails reconstruction of the time-dependent trajectory of a conventional time-resolved growth curve, and whether it is sufficiently robust in relation to the degree of physiological and metabolic agreement of cell cultures cultivated in separate wells with increasing dilutions, is still under-described. Moreover, it is also not clear whether reliable quantification of assimilation and secretion profiles of compounds from simple and complex mixtures of carbon sources can be made. Establishing the dilution-resolved method as gold standard platform for high-throughput metabolomic analyses would, therefore, be a step forward in connection with both biotechnological applications and automation purposes.

Here, we applied both time-resolved and dilution-resolved methods for metabolic footprinting analyses of the model species *P. putida* KT2440 and *P. aeruginosa* PAO1. Since most biotechnological applications rely on inexpensive and simple carbon sources, we analysed *P. putida* KT2440 when growing in the presence of glucose as an archetypal sugar substrate. In contrast, *P. aeruginosa* PAO1 was analysed when growing in the defined rich Synthetic Cystic Fibrosis Medium (SCFM) that reproduces the CF lung milieu, thereby, representing the nutrient composition relevant for an infection. Comparative analyses demonstrated that the dilution-resolved method produces metabolic footprinting data from both simple and complex media, similar to those produced by the conventional time-resolved method. Moreover, this approach provides flexibility as it can fulfil diverse experimental needs by merely changing the cultivation set-up, therefore, supporting its use for high-throughput

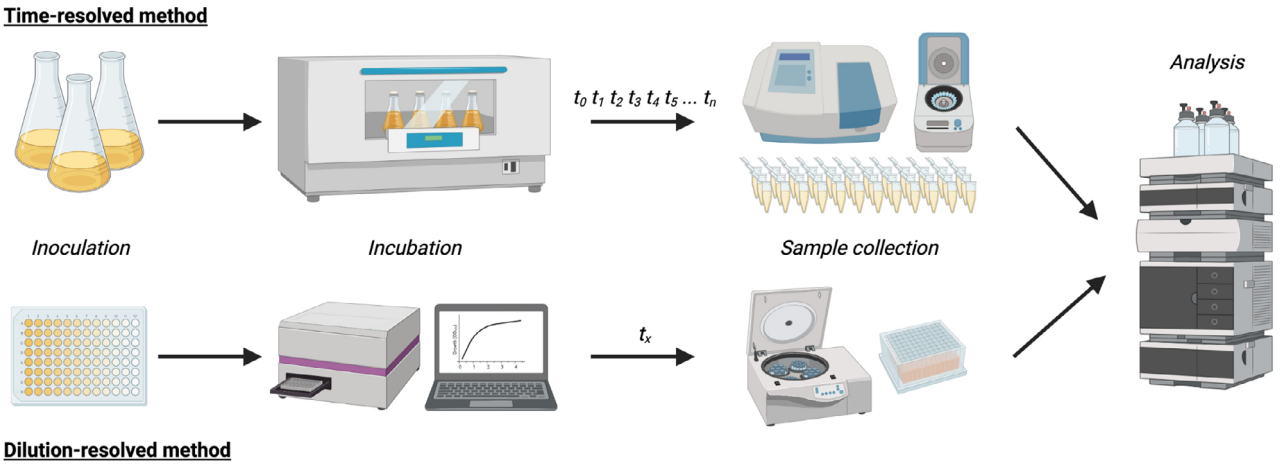

Fig. 1. Schematic representation of the time-resolved and dilution-resolved workflow for exo-metabolomic analyses. For the time-resolved method, bacteria are cultivated in Erlenmeyer flasks and incubated in a flask shaker incubator. Samples are collected over time (t_1 t_2 t_3 t_4 t_5 ... t_n) for OD measurement to follow bacterial growth and supernatants are collected by centrifugation. For the dilution-resolved method, bacteria are inoculated in 96-well plates in serial dilutions and incubated in a microtiter plate reader to follow the growth in real time. At the time of sampling (t_x), all supernatant samples are harvested simultaneously by centrifugation.

screening of large collections of strains and/or growth conditions.

Results and discussion

Sampling by time-resolved and dilution-resolved methods provide comparable sample distributions

Dilution-resolved growth curves in 96-well deep-well plates and microtiter plates were compared with conventional time-resolved growth curves from continuous sampling over time from Erlenmeyer flasks to compare the distribution of the collected samples. *P. putida* KT2440 was cultivated in de Bont minimal medium (Hartmans *et al.*, 1989) with glucose as sole carbon source and *P. aeruginosa* PAO1 in the defined rich SCFM medium containing amino acids, glucose and lactate as carbon and nitrogen sources (Palmer *et al.*, 2007). *P. putida* was cultivated in Erlenmeyer flasks, 96-well deep-well and microtiter plates, while *P. aeruginosa* was only cultivated in Erlenmeyer flasks and 96-well deep-well plates. Many clinical isolates of *P. aeruginosa* create free-floating bacterial aggregates in microtiter plates which interfere with the optical density (OD) acquisition and, therefore, producing unreliable measurements. Moreover, while production strains are routinely screened in microtiter plates, few large-scale screenings have been performed with clinical isolates in microtiter plates (Wewetzer *et al.*, 2015; Kragh *et al.*, 2018; Bartell *et al.*, 2019). For these reasons, we excluded microtiter plates for *P. aeruginosa* analyses and focussed only on deep-well plates and flasks. Dilution-resolved plates were prepared by serial dilutions of overnight cultures of *P. putida* in fresh de Bont minimal medium and of *P. aeruginosa* in fresh SCFM. To adequately cover the growth phases of interest, the dilution factor, the number of dilutions, the inoculum density and the incubation time must be chosen appropriately. The dilution factor, together with the number of dilutions, controls the growth time-shift between the cultures, while the incubation time, together with the inoculum density, controls the range of ODs at which the cultures are sampled. Changing either the dilution factor or the inoculum density makes it possible to carry out the cultivations by the incubation time which best suits the specific needs. To describe two very different approaches and assess the adaptability of the method, we selected a low inoculum density and a long incubation time for *P. putida* and a high inoculum density and a short incubation time for *P. aeruginosa*. It should be noted that while quantification of sugars by HPLC is inexpensive and widely accessible, amino acid quantification is still more costly and requires an *ad hoc* set-up due to the complexity of the amino acid chemistry. For this reason, for *P. putida* we prioritized a high resolution of the growth curve, whereas for *P. aeruginosa*, we reduced the number of dilutions to a minimum, which could provide full coverage of the growth curve.

For *P. putida*, a low inoculum density with OD_{600} values (OD at 600 nm) between 5.0×10^{-2} and 9.5×10^{-8} and an array of 20 serial dilutions was used (Fig. 2A). For *P. aeruginosa*, a high inoculum density with OD_{600} between 2.0×10^{-1} and 3.9×10^{-4} and an array of 8 serial dilutions was used (Fig. 2B). A dilution factor of 1:2 was applied for both strains (see Experimental Procedures for a full description of the method). To produce time-shifted cultures mirroring 12 and 9.5 h of bacterial growth in conventional Erlenmeyer flasks, an

incubation time of 22 h for *P. putida* and 5.5–6.5 h for *P. aeruginosa* was required (Fig. 2). Independently of the specific set-up and strain, the distribution of the OD values of the samples collected using the dilution-resolved method showed coverage of ODs similar to the conventional time-resolved growth curves (*Z*-score range = 0.08–0.23) (Fig. 2).

These results suggest that the samples collected using the high-throughput dilution-resolved method can capture the same growth states as in the time-resolved method. Moreover, they confirm the relationship between lag phase and cell density at any given time for the strains and laboratory conditions used in this study, indicating robustness and simultaneous flexibility of the dilution-resolved method in the presented experimental set-up and with the specific analysed strains. Importantly, the relationships between inoculum density, dilution factor and incubation time should be specifically explored for each combination of media condition, numbers of samples required, and specific bacterial strains in order to identify the optimum conditions.

The dilution-resolved method captures the different phases of initial glucose processing in P. putida

For applications of the dilution-resolved method, it is important that the relationship between the metabolomes of the different cultures growing in different wells, progressively diluted, is analogous to the relationship between the metabolomes of a single culture sampled continuously over time. The metabolite concentration in supernatant samples from both time-resolved and dilution-resolved methods should, therefore, change similarly maintaining a linear relationship between the samples. To test this possibility, supernatant samples collected from *P. putida* cultures, established using the dilution-resolved method, were analysed by HPLC to quantify glucose metabolism intermediates, and compared to samples collected using the time-resolved methods (Fig. 2A). Regardless of the method used and the cultivation set-up (flask, deep-well or microtiter plates), the relationship between the samples, that is the relationship between the metabolites abundance and the OD, was maintained, making it possible to determine profiles of assimilation and secretion for glucose, GA and 2-KGA (Fig. 3A and Table S1). In all cases, glucose was assimilated during the entire cultivation while GA and 2-KGA were initially secreted and catabolized by the cells at later stages during late exponential and stationary phase. Interestingly, the cultivation set-up imposed a specific metabolic constraint, resulting in slightly different assimilation and secretion profiles. While the maximal concentration of GA was comparable between the cultivation setups (~3.2 mM), the growth phase at which it was secreted varied between flask and deep-well plate (exponential phase) and microtiter plate (stationary phase) (Fig. 3A). 2-KGA was detected only in flask cultures and deep-well plates, although secretion occurred

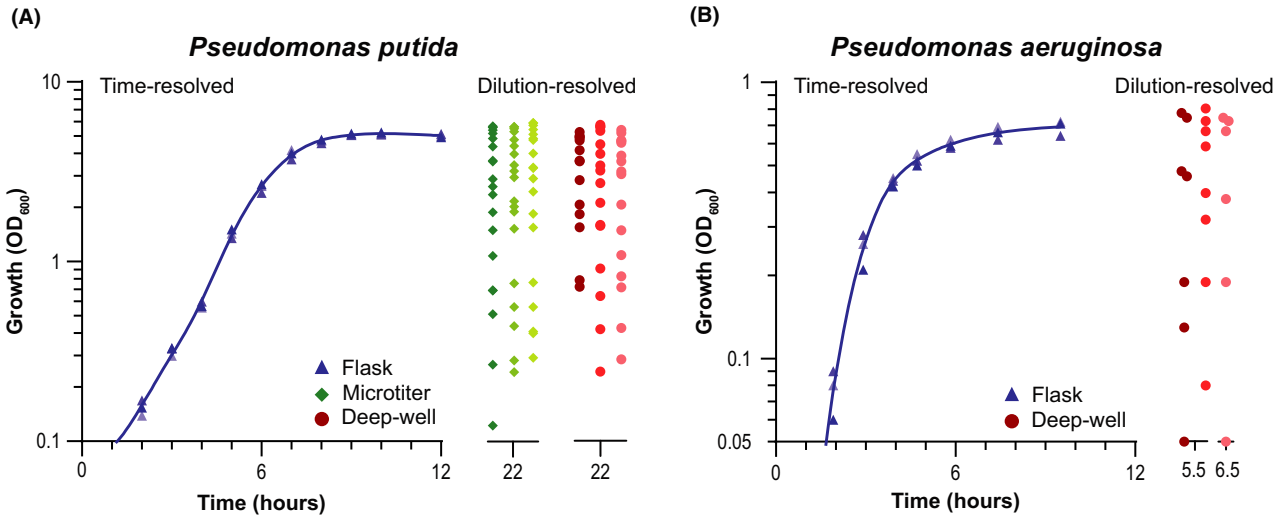

Fig. 2. Time-resolved and dilution-resolved growth curves of *Pseudomonas putida* and *Pseudomonas aeruginosa*.
A. Growth curve and distribution of samples of *P. putida* cultivated in de Bont minimal medium in the presence of glucose in Erlenmeyer flasks (blue symbols and lines), deep-well plates (red symbols) and microtiter plates (green symbols).
B. Growth curve and distribution of samples *P. aeruginosa* cultivated in SCFM in Erlenmeyer flasks (blue symbols and lines) and deep-well (red symbols) plates. Each symbol represents a sample collected during the growth using the time-resolved method (blue symbols) or at incubation time using the dilution-resolved method (red and green symbols). Shades of colour represent three independent biological replicates. For comparison, the distribution of the samples collected using the dilution-resolved method is shown at the side of each graph. Time-resolved growth curves were inferred by fitting a spline/LOWESS curve to the OD_{600} (OD at 600 nm) and time data.

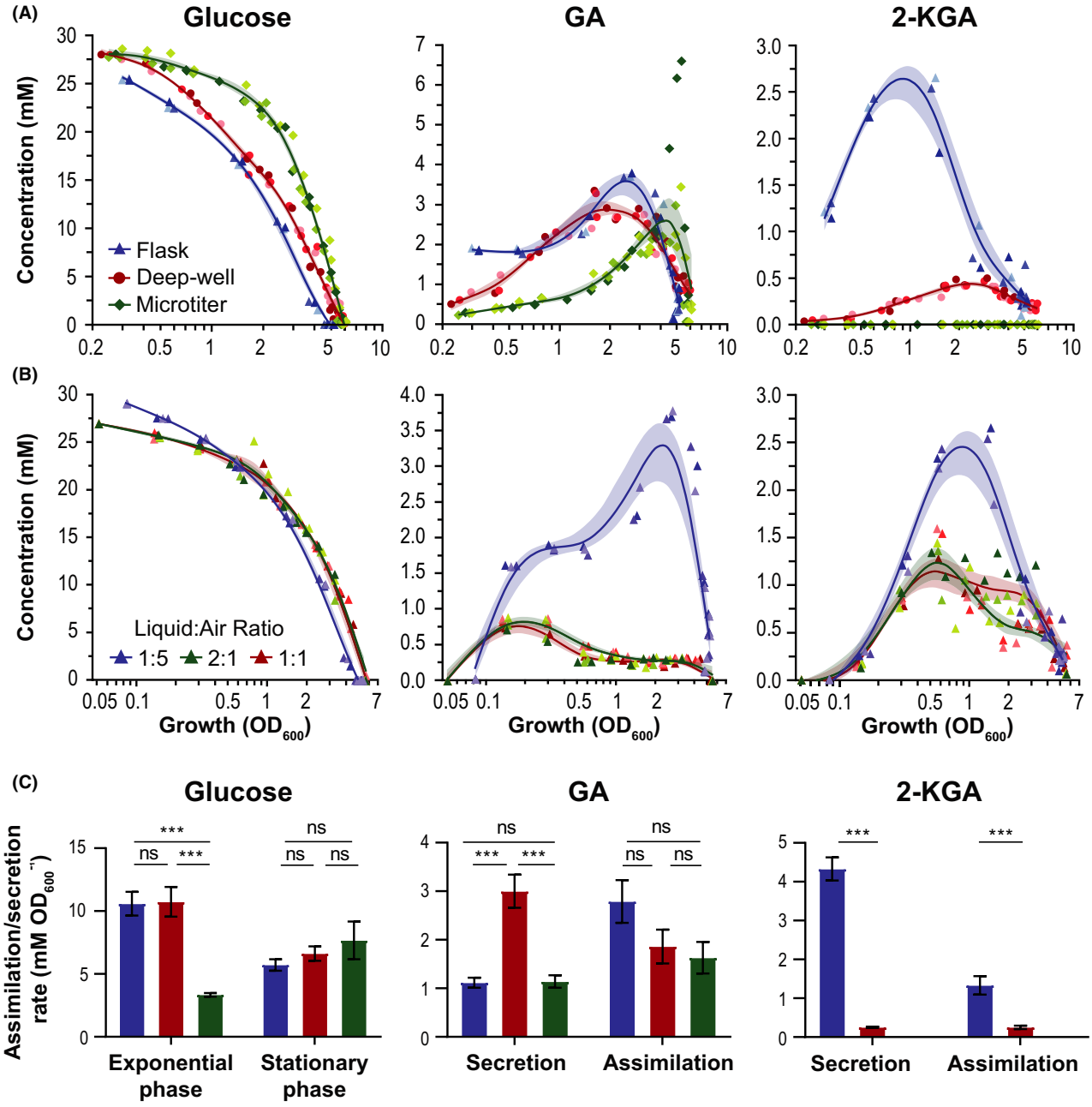

Fig. 3. Dynamics of sugar uptake and its conversion into oxidized products in *P. putida*.
A. The concentration of glucose, gluconate (GA) and 2-ketogluconate (2-KGA) in Erlenmeyer flasks (blue symbols and lines), deep-well plates (red symbols and lines) and microtiter plates (green symbols and lines) is shown relative to the OD_{600} (OD at 600 nm) at which supernatant samples were collected. The time-resolved method was used for cultivation of *P. putida* in Erlenmeyer flasks while the dilution-resolved method for deep-well and microtiter plates in de Bont minimal medium in the presence of 27.7 mM of glucose as sole carbon source. Shades of colour represent three independent biological replicates while shaded areas indicate the 95% confidence intervals of the curves (cubic spline fitting).
B. Concentration of glucose, gluconate and 2-ketogluconate in Erlenmeyer flasks in de Bont minimal medium in the presence of 27.7 mM of glucose as sole carbon source at ratios of culture media to air volume of 1:5 (blue symbols and lines), 1:1 (red symbols and lines) and 2:1 (green symbols and lines) relative to the OD at which supernatant samples were collected. Shades of colour represent three independent biological replicates while shaded areas indicate the 95% confidence intervals of the curves (cubic spline fitting).
C. Maximal assimilation and secretion rate for glucose, gluconate and 2-ketogluconate in Erlenmeyer flasks (blue bars), deep-well plates (red bars) and microtiter plates (green bars). Parameters were calculated by linear regression from the six samples that produced the highest rate. For glucose, assimilation rate was calculated during both exponential and stationary phase. The error bar indicates the SEM (Standard Error of the Mean). Differences between rates were evaluated by Unpaired Welch *t*-test with significance indicated as 'ns' where $P > 0.05$, and '***' where $P < 0.001$.

at later time points and at lower concentration (fivefold reduction; Fig. 3A). No 2-KGA was identified in microtiter plate cultures. We hypothesize that limited oxygen availability in multi-well plates, mostly due to the different ratios between medium and air volume (1:5 for flasks, 1:1 for deep-well plates, and 2:1 for microtiter plates) and the different oxygen-transfer rate (OTR) between setups, led to reduced 2-KGA formation (Duetz and Witholt, 2004; Wewetzer *et al*., 2015). Oxygen is an important factor for glucose assimilation, and if limited may cause rearrangement of the metabolite fluxes within the glucose catabolic pathway (Davis *et al*., 2015). To substantiate this hypothesis, we quantified the glucose, GA and 2-KGA assimilation and secretion profiles in flasks using a ratio of medium versus air of 1:1 and 2:1 and compared it with the 1:5 set-up (Fig. 3B). Glucose assimilation pattern overlapped between conditions, while GA showed a threefold reduction relative to the 1:5 set-up and it was secreted only during early exponential phase in both 1:1 and 2:1 flasks (Fig. 3B). Moreover, while in microtiter plates no 2-KGA was identified, in the corresponding 2:1 flask set-up, 2-KGA was still secreted albeit at lower concentration (twofold reduction) (Fig. 3B). This indicates that in our experimental set-up, oxygen availability is still higher in flasks relative to deep wells and microtiter plates due to the different OTR which ultimately depends on the shape and size of the vessel, on the orbital diameter and on the rate of shaking (Duetz and Witholt, 2004; Wewetzer *et al*., 2015).

Maximal rates of glucose consumption and secretion of GA and 2-KGA, computed at the six OD points that produced the highest rates, deviated between the methods as a consequence of the different cultivation setups (Fig. 3C and Table S1). While the specific glucose consumption rate was similar in flasks and deep-well plates, it was threefold lower in microtiter plates during exponential phase (Unpaired Welch *t*-test) (Fig. 3C). For GA, there was no significant difference between the assimilation rates using the different methods, but its secretion rate was 2.7-fold higher in deep-well plates (Unpaired Welch *t*-test) (Fig. 3C). For 2-KGA, both assimilation and secretion rates differed significantly between the methods (Unpaired Welch *t*-test) as also shown by the secretion plot (Fig. 3A).

Regardless of the underlying regulatory mechanism, it is worth noting that the cultivation set-up should be taken into account while planning high-throughput experiments using the dilution-resolved method. Indeed, OTR should be specifically analysed to match the desired oxygen availability for the specific cultivation (Duetz, 2007). Parameters such as cultivation volume, shape of the vessel, orbital diameter and rate of orbital shaking can be specifically selected to perfectly match the desired final cultivation set-up. Nonetheless, these results confirm the reliability of the method for analyses of targeted metabolites assimilated or secreted during bacterial cultivations in the presence of a single carbon source.

P. aeruginosa's *complex metabolic behaviour in SCFM is maintained irrespective of the cultivation method*

To further test whether the dilution-resolved method can be applied to assess complex metabolic patterns from a rich defined complex medium such as SCFM, the supernatant samples collected from *P. aeruginosa* cultivations using both the dilution-resolved and time-resolved methods (Fig. 2B), were analysed by targeted exo-metabolomics and compared with respect to changes in metabolite composition over time and dilution.

Performing a Principal Component Analysis (PCA), which explains 89% of the variance on PC1, shows how the exo-metabolomes overlap between the two sampling methods and follow the same trajectory as a function of growth and metabolite assimilation (Fig. 4A). Similarly, a hierarchical clustering analysis (HCA) of the variance of each specific metabolite, summarizing the reduction in concentration across all samples of a given experiment, shows a mixed clustering of the experiments regardless of the sampling method (Fig. 4B). Compounds such as aspartic acid, glutamic acid, proline, alanine, arginine and serine show the highest variance being assimilated during the early stages of growth. The remaining compounds, in contrast, show low variance since they were not assimilated in the analysed growth window (Fig. 4B and Fig. S1). It should be pointed out that for *P. aeruginosa*, samples were collected mainly during exponential and early stationary growth phase to maximize the resolution of the most preferred carbon sources. Therefore, to cover the assimilation profiles of the remaining compounds, a higher number of dilutions or a higher dilution factor should be selected. Similar to what was shown for *P. putida*, assimilation curves overlapped using the two methods, both for the fully (aspartic acid), partially (proline) and not (tyrosine) assimilated compounds without showing significant differences based on the cultivation method (Fig. 4C, Fig. S1 and Table S1).

To further investigate whether the hierarchy and rates of assimilation were similar between methods, we fitted mechanistic growth models and linear regression models to the data of the seven metabolites, which were either completely or partially assimilated during the exponential growth phase (Fig. 4D and E and Table S1). The mechanistic growth model allows quantifying important parameters such as the metabolite half-life (OD_{50} value), which represents the OD at which 50% of a compound has been assimilated. When metabolites are ordered by their OD_{50} value, the hierarchy of assimilation can be defined

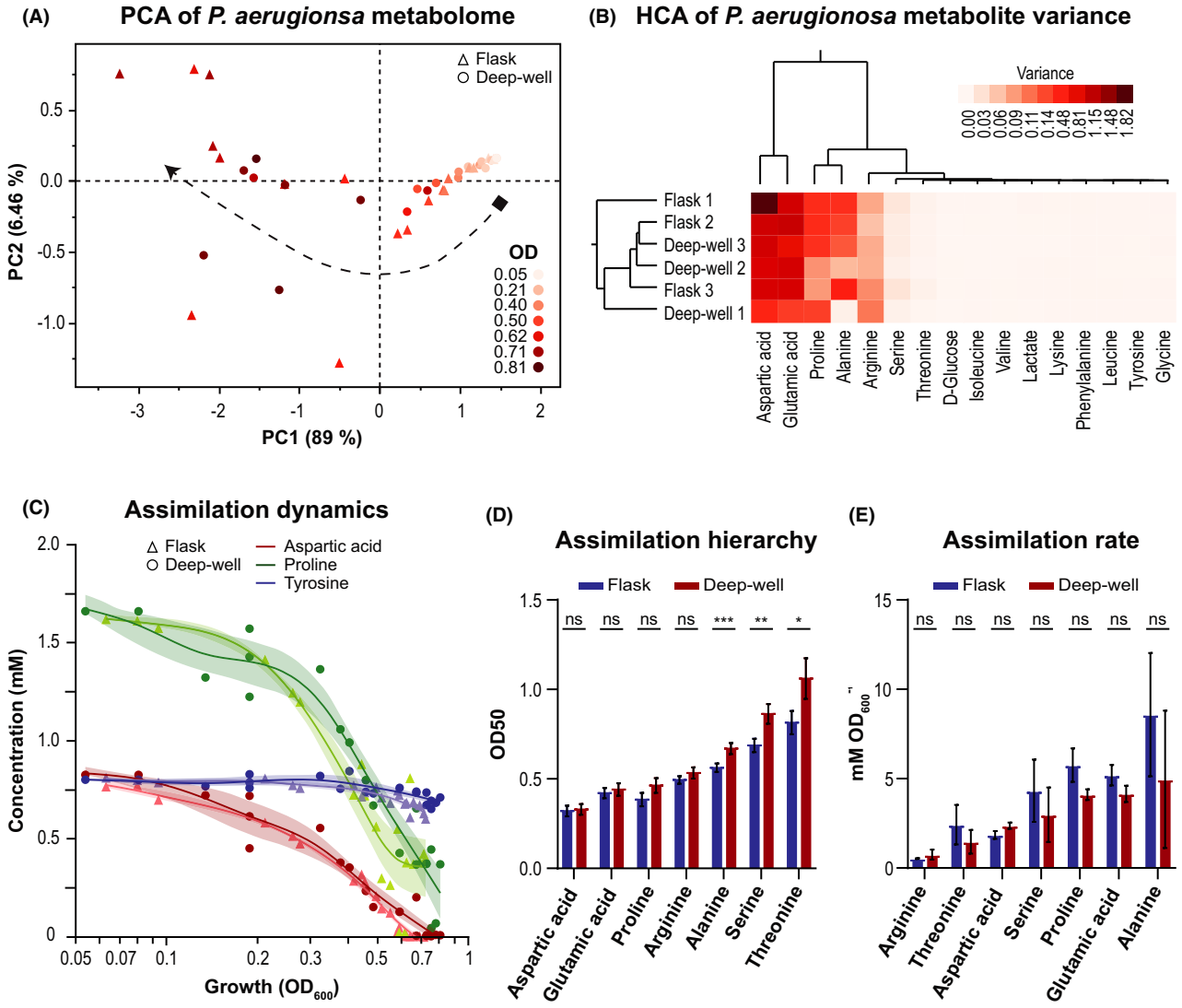

Fig. 4. Metabolism dynamics of *Pseudomonas aeruginosa* cultivated in SCFM rich medium.
A. Principal Component Analysis (PCA) of the exo-metabolomes of *P. aeruginosa* collected using the time-resolved (triangles) and dilution-resolved methods (circles). Dots represent the metabolome of each supernatant sample at a given OD. The OD is represented by a colour gradient and the black dashed arrow indicates the trajectory of the metabolome during growth.
B. Two-way hierarchical cluster analysis (HCA) of the quantified metabolites grouped by cultivation methods and metabolite dynamics. The heat map shows the variance of the concentration of each compound which is a proxy of the shift in metabolite concentration within the samples of a specific method. Compounds with higher variance are assimilated earlier than those with lower variance. Compounds not assimilated show null variance.
C. Assimilation of aspartate (red lines and symbols), proline (green lines and symbols) and tyrosine (blue lines and symbols) during cultivation using either the time-resolved (triangles) or the dilution-resolved (circles) method in Erlenmeyer flasks and deep-well plates respectively. The plot shows examples of metabolites completely assimilated (aspartate), partially assimilated (proline) and not assimilated (tyrosine) by *P. aeruginosa* when growing in SCFM respectively. Shaded areas indicate the 95% confidence intervals of the curves (cubic spline fitting).
D and E. Assimilation parameters of the compound uptaken during exponential growth. The maximal assimilation rate was calculated by fitting a linear regression model to the five data points which showed the highest reduction in concentration. The hierarchy of assimilation was defined by ordering the assimilated metabolites by their half-life (OD_{50}), which represents the OD at which the concentration of each compound halved. The OD_{50} were calculated by fitting a mechanistic growth model to the metabolite's concentration relative to the OD. The error bar indicates the SEM (Standard Error of the Mean). Differences between rates were evaluated by Unpaired Welch *t*-test with significance indicated as 'ns' where $P > 0.05$, '*' where $P < 0.05$, '**' where $P < 0.01$ and '***' where $P < 0.001$.

based on the cellular metabolic preference (Behrends *et al.*, 2014). When comparing the OD_{50} values between methods, no statistical differences (Unpaired Welch *t*-test) were shown for the four most preferred carbon sources. Although the latter three showed some small differences between methods, the hierarchy is clearly preserved, supporting the constancy of the hierarchy of assimilation in SCFM (Fig. 4D and Table S1). Similarly, the assimilation

rates were comparable between methods confirming the reliability of the dilution-resolved method for the characterization of complex metabolic behaviours (Fig. 4E and Table S1). Interestingly, even using only the data of two biological replicates, the hierarchy and the rates of assimilation were comparable, irrespective of the method, confirming the robustness and the potential of the dilution-resolved method (Fig. S2 and Table S1).

Opposite to what was shown for *P. putida*, no considerable difference in assimilation profiles was observed when using the two cultivation methods (flask versus deep-well). The OD_{50} assimilation hierarchy of PAO1 has been previously described in LB medium (La Rosa *et al*., 2018). Arginine was not identified in that study, but the order of assimilation for the remaining six preferred metabolites is identical between studies, indicating a common metabolic preference of *P. aeruginosa* PAO1, independent of the growth medium.

Altogether, these results show that metabolism is conserved in individual wells in the high-throughput dilution-resolved method, reflecting changes in the metabolome composition during growth, as accurately as in the time-resolved method. Moreover, it suggests that complex patterns of metabolic behaviour are maintained independent of the cultivation set-up and/or sampling method.

Discussion

Metabolic characterization of bacterial strains is usually carried out in a low-throughput manner, which is time and resource consuming. Only a limited number of high-throughput methods are available (Zampieri *et al*., 2017), mostly devoted to strain characterization towards biotechnological applications. Here, we have shown that a dilution-resolved method for dynamic sugars quantification and targeted exo-metabolomic analysis is both robust and flexible. Indeed, independently of the specific species and cultivation set-up, the relationship between the metabolic and physiological status of cell cultures progressively diluted cultivated accordingly to the dilution-resolved method is maintained. Parameters such as cultivation set-up, dilution factor, number of dilutions, inoculation density and incubation time can be tuned to the specific metabolic dynamics of the cells or to specific needs of the operator, providing flexibility and optimal solutions for customization. This method can easily become integrated in automated workflows using liquid-handling robots with applications that include biotechnology platform strains such as *P. putida* but also clinically relevant isolates as *P. aeruginosa*. The method can be used for both high-resolution investigations by increasing the number of dilutions per strain/condition, and for large-scale high-throughput investigations by increasing the dilution factor and reducing the number of dilutions per strain/condition. Moreover, by modifying either the dilution factor or the inoculum density, the cultivation can be carried out using both short and long incubation times which allows even more flexibility. While scalability using the time-resolved method depends on the availability of the laboratory resources (flasks, incubators, etc.), the dilution-resolved method can be easily scaled up to 96 samples using multi-well plates and a single laboratory set-up. Since the set-up of bacterial cultivation has an impact on the exo-metabolite dynamics as a consequence of the different cellular physiology, it should be considered when planning high-throughput experiments using the dilution-resolved method. OTR, indeed, varies between cultivation vessels and setups and it should, therefore, be specifically selected in relationship to the oxygen requirement for the cultivation. Matching the metabolic profiles of bacteria growing in microtiter plates in simple carbon sources to the flask condition, therefore, requires further optimization. Scalability of microtiter plates to larger fermenters indeed poses several challenges which have been previously investigated (Duetz, 2007). However, overall in our experiments with Pseudomonads, deep-well plates provided the best cultivation conditions which are comparable to Erlenmeyer flasks and which permit analysis of large numbers of strains and/or culture conditions in a high-throughput manner. Further validation and optimization are required for other industrially or biologically relevant species. Although the dilution-resolved method in the present study was only applied for high-throughput sampling for dynamic sugar quantification and for targeted exo-metabolomic analyses, it can also be optimized for endo-metabolomic analysis and for transcriptomic, fluxomic or proteomic analyses with relatively few adjustments. Whether the dilution-resolved data are in agreement with the time-resolved data, however, merits further investigations. Still, the method has been successfully used for quantification of rhamnolipids in *P. aeruginosa* and production of biofilm in *P. putida* (van Ditmarsch and Xavier, 2011; López-Sánchez *et al*., 2013). Importantly, the relationship between the diluted cell cultures is linear between different wells, indicating that the metabolic processes, controlled by several global and local regulators, are maintained independent of the initial inoculum. In conclusion, the dilution-resolved method can be combined with exo-metabolomics as a powerful tool for high-resolution and/or high-throughput metabolic footprinting investigations of bacteria with complex metabolic dynamics.

Experimental procedures

Bacterial strains and media composition

Pseudomonas putida KT2440 was cultivated in de Bont minimal medium (containing, per litre of final medium,

1.55 g K_2HPO_4, 0.85 g NaH_2PO_4, 2.0 g $(NH_4)_2SO_4$, 0.1 g $MgCl_2$, 10 mg EDTA, 2 mg $ZnSO_4$, 1 mg $CaCl_2$, 5 mg $FeSO_4$, 0.2 mg Na_2MoO_4, 0.2 mg $CuSO_4$, 0.4 mg $CoCl_2$, and 1 mg $MnCl_2$) containing 5 g/L (27.7 mM) of glucose as sole carbon source. de Bont minimal medium was prepared according to (Hartmans *et al*., 1989) and a single medium batch was used for all the experiments to avoid any differences that could arise from medium composition. *Pseudomonas aeruginosa* PAO1 was cultivated in the defined rich medium Synthetic Cystic Fibrosis Medium (SCFM), designed to mimic the conditions of the airways in patients with cystic fibrosis and containing amino acids, glucose and lactate as carbon sources (Turner *et al*., 2015). We excluded DNA and mucins to reduce viscosity and allow HPLC analysis of the samples (Deschamps *et al*., 2021). Two different batches of SCFM were used for the cultivation experiments in deep-well plates and Erlenmeyer flasks, respectively, and some variation in the concentration of specific metabolites was determined by HPLC analysis. These differences are listed in Table S1. *P. putida* was cultivated in baffled Erlenmeyer flasks, 96-well deep plates (Cat. No. 0030502302; Eppendorf, Hamburg, Germany) and 96-well clear bottom microtiter plates (Cat. No. 650001; Greiner Bio-One, Kremsmünster, Austria) while *P. aeruginosa* in baffled Erlenmeyer flasks and 96-well deep plates. In all cases, both precultures and cultures were incubated in the same culture medium to avoid changes in media composition and extended lag phase. *P. putida* precultures were carried out overnight in 50-ml Falcon tubes containing 10 ml of de Bont medium containing 5 g/L (27.7 mM) of glucose as sole carbon source at 250 rpm at 30°C. *P. aeruginosa* precultures were carried out overnight in 15-ml Falcon tubes containing 6 ml of SCFM at 250 rpm and at 37°C. For both species, a shaker incubator with an orbit diameter of 2.5 cm (1 in) was used.

Time-resolved cultivation method

For the time-resolved method, bacteria were cultivated in Erlenmeyer flasks in three independent biological replicates. Precultures of *P. putida* were grown for 18 h, centrifuged at 10 000*g* for 5 min, washed twice in 1-ml de Bont medium without glucose and used to inoculate at OD_{600} of 0.05, 250-ml Erlenmeyer flasks containing 50 ml (1:5 media to air volume ratio), 125 ml (1:1 media to air volume ratio) or 166.7 ml (2:1 media to air volume ratio) of glucose de Bont medium. During cultivation at 30°C and 200 rpm, 0.5 ml of bacterial culture was harvested after 2, 3, 4, 5, 6, 7, 8, 9, 10 and 12 h, the OD_{600} recorded, and the supernatant collected by centrifugation at 21 000*g* for 5 min at 4°C. Samples were stored at −20°C until further analysis. Precultures of *P. aeruginosa* were grown overnight and directly used, without washing, to inoculate at 0.05 of OD_{600}, 100-ml Erlenmeyer flasks containing 50 ml of SCFM. During cultivation at 37°C and 250 rpm, 1 ml of bacterial culture was harvested after 2, 3, 4, 4.75, 5.75, 7.5 and 9.5 h of incubation, the OD_{600} recorded, and the supernatant collected by centrifugation at 21 000*g* for 7 min at 4°C. Samples were stored at −80°C until further analysis. For both species, a shaker incubator with an orbit diameter of 2.5 cm (1 in) was used.

Dilution-resolved cultivation method

For *P. putida*, three independent overnight cultures were washed as for the time-resolved method and inoculated at OD_{600} of 0.05 in a 96-well deep plate containing 1 ml of de Bont medium in rows B, C and D of column 2 and diluted sequentially 1:2 until column 11, and again from rows E, F and G of columns 2 till column 11. This way an array of 20 dilutions was established for each biological replicate. Columns 1 and 12 were used as contamination control and contained de Bont medium with glucose. 96-well microtiter plates were set up similarly to the deep-well plates with few differences. The volume of cultivation was set to 200 μl and since growth was performed without the plate lid to avoid condensation, the remaining external wells were filled with 280 μl of water to reduce evaporation which in all cases was on average 9.7 ± 3.7%. For *P. aeruginosa*, a different approach was used. Three independent overnight cultures were used directly without washing to prepare two master culture dilutions at the OD_{600} of 0.25 and 0.00625 and used to inoculate wells from columns 1 to 6 and 7 to 11 respectively. In this way, specific volumes of each master dilution (960, 480, 240, 120, 60 and 30 μl from dilution 1 and 600, 300, 150, 75 and 38 μl from dilution 2 respectively) were used to inoculate each well of a deep-well plate, after which the corresponding volume of SCFM was added to reach a final volume of 1.2 ml. On average, the amount of carry-over of preculture medium was 1.7% ± 3.4%. However, no amino acids, sugars or organic acids were identified in the overnight precultures. Column 1 was inoculated at an initial OD_{600} of 0.2 and the following columns corresponded to 1:2 dilutions. Column 12 was used as contamination control and contained pure SCFM. In both cases, deep-well plates were incubated at 30°C (*P. putida*) or 37°C (*P. aeruginosa*) in an orbital shaker with an orbital diameter of 2.5 cm (1 in) at 250 rpm. After 22 h (*P. putida*) and 5.5-6.5 h (*P. aeruginosa*), when the wells of the second-lowest dilution showed signs of growth, 40 μl of cell suspensions were transferred to a new 96-well microtiter plate to measure the OD_{600} in a Synergy™ MX microtiter plate reader (BioTek Instruments Inc., Winooski, VT, USA).

The remaining volume was centrifuged at 1740*g* at 4°C for 30 min to separate the biomass from the supernatant (250 μl) which was stored at −20°C (*P. putida*) or −80°C (*P. aeruginosa*) until further analysis. 96-well microtiter plates for *P. putida* cultivation were incubated at 30°C in a BioTek® ELx808 Absorbance Microtiter Reader (BioTek Instruments Inc., Winooski, VT, USA) where the shake movement is a repeated 0.021 inch (0.05334 cm) movement from the shake position and back. The shaking mode was set to 'medium' mode which corresponds to 18 Hz or approximately 1080 rpm. The bacterial growth was followed by measuring the OD_{630} every 15 min. After 22 h of growth, 150 μl of each well was transferred to a 96-filter plate ($MultiScreen_{HTS}$, HV Filter Plate 0.45 μm, hydrophilic, clear, non-sterile, Millipore, Catalogue number MSHVN45) to filter out the bacteria and collect the supernatants. Plates were centrifuged at 1000*g* for 3 min and the supernatants stored at −20°C until further analysis. For each experiment, 16 to 20 samples/time points for *P. putida* and 6 to 8 samples/time points for *P. aeruginosa* were selected for HPLC analysis based on the following criteria: (i) the OD reflected the dilution relative to the other samples; and (ii) the total samples provided the highest variance of ODs.

High-performance liquid chromatography for sugars quantification and targeted exo-metabolomic analysis

For sugars analyses and targeted exo-metabolomic analyses, frozen samples were thawed at 4°C and further processed for high-performance liquid chromatography (HPLC). Glucose, gluconate and 2-ketogluconate concentration, for the *P. putida* experiments, were quantified on a Dionex Ultimate 3000 system (Thermo Scientific, Waltham, USA) with a HPx87H ion exclusion column (125-0140, Aminex, Dublin, Ireland), equipped with a guard column (125-0129, Bio-Rad, Hercules, California, USA) and guard column holder (125-0131, Bio-Rad, Hercules, California, USA) and eluted with 5 mM H_2SO_4 at an isocratic flow of 0.6 ml min^{-1} at 30°C for 30 min. Glucose and 2-ketogluconate were analysed by RI detection using a Smartline RI detector 2300 (KNAUER Wissenschaftliche Geräte, Berlin, Germany), whereas gluconate was analysed by UV detection at a wavelength of 210 nm using a System Gold 166 UV detector (Beckman Coulter, Brea, USA). Metabolites for the *P. aeruginosa* experiments were quantified using two separate HPLC methods. Organic acids and sugars (glucose, gluconate, succinate, lactate, formate, acetate and pyruvate) were analysed by the same methodology and instrument as for *P. putida*, but at 45°C instead of 30°C. Pyruvate was analysed by UV detection while all other organic acids and sugars were analysed by RI detection.

For amino acids quantification (aspartic acid, glutamic acid, cysteine, asparagine, serine, glutamine, histidine, glycine, threonine, arginine, alanine, tyrosine, valine, methionine, tryptophan, phenylalanine, isoleucine, leucine, lysine and proline), 20 μl of supernatant sample was diluted 1:10 in Ultrapure MilliQ water and mixed with 100 μl of internal standard (20 μg/ml 2-aminobutyric acid and sarcosine). Derivatization was performed directly in the HPLC-instrument prior to injection by automatic mixing with the following eluents: (i) 0.5% (v/v) 3-mercaptopropionic acid in borate buffer 0.4 M at pH 10.2; (ii) 120 mM iodoacetic acid in 140 mM NaOH; (iii) OPA reagent (10 mg/mL *o*-phthalaldehyde and 3-mercaptopropionic acid in 0.4 M borate buffer); (iv) FMOC reagent (2.5 mg/ml 9-fluorenylmethyl chloroformate in acetonitrile); and (v) buffer A (40 mM Na_2HPO_4, 0.02% (w/v) NaN_3 at pH 7). After derivatization, samples were separated isocratically on a Dionex UltiMate 3000 HPLC with fluorescence detector (Thermo Scientific, Waltham, USA) through a Gemini C18 column (00F-4439-E0, Phenomenex, Værløse, Denmark) equipped with a SecurityGuard Gemini C18 guard column (AJ0-7597, Phenomenex, Værløse, Denmark) with a flowrate of 1 ml/min at 37°C using a 5 mM sulfuric acid mobile phase. Metabolites were detected using an UltiMate™ 3000 Fluorescence variable wavelength UV detector (FLD-3400RS, Waltham, Massachusetts, USA). Standard curves for each metabolite were used for absolute quantification. All chromatograms were analysed using the software Chromeleon v7.2.9.

Data analysis

Compounds which signal was undetectable (pyruvate, gluconate, formate, succinate and acetate), near the detection limit in all samples (asparagine and glutamine), if a reliable calibration was not possible due to instability of the metabolite (cysteine) or if signal appeared in blanks (tryptophan and methionine) were excluded from the analysis. Missing values were replaced with 20% of lowest detected concentration (mM). Since different batches of SCFM were used for cultivation in flasks and deep-well plates with slight variations in the specific metabolites concentration, they were normalized to percentage and then recalculated setting as 100% of the metabolite concentration of the SCFM standard formulation (see Table S1). For principal component analysis (PCA) and hierarchical clustering analysis (HCA), the metabolite concentration was normalized by $\log_{10}$ transformation. PCA was calculated on the covariance of each metabolome (sample/time point). HCA was calculated using Ward's method on the variance of the concentration of each metabolite, which shows how much the concentration of each metabolite varies across

samples. To calculate the metabolites OD_{50}, which represent the OD at which 50% of the metabolite has been assimilated (metabolite half-life), the concentrations were plotted against the $\log_{10}$(OD) and several sigmoidal models (Gompertz 3P and 4P, Logistic 4P, 4P Hill and 5P, Probit 4P and Mechanistic Growth) and exponential models were fit to the assimilation profiles. The mechanistic growth model (Equation: $a(1-b\text{Exp}(-cx))$ where a = asymptote, b = scale and c = rate) was selected because it provided the best fit across AICc, AICc Weight, BIC, SSE, MSE, RMSE and R^2 parameters, as well as producing the lowest standard error for OD_{50} across metabolites. The hierarchy of assimilation for *P. aeruginosa* was identified by ordering the assimilated compounds by their OD_{50}. The assimilation rate was calculated from a minimum of five points by linear regression, and it was limited to samples in the OD range that produced the highest rate. Statistical significance between OD_{50} values and assimilation rates was determined by Unpaired Welch *t*-test. Data analyses were carried out using the software JMP® version 15, except for Welch *t*-test, which was computed in GraphPad Prism 9.0. Time-resolved growth curves were inferred by fitting a spline/LOWESS curve with 9 knots for *P. putida* and 8 knots for *P. aeruginosa* to the OD and time data using GraphPad Prism 9.0. Bar charts were created in GraphPad Prism 9.0 and the schematic in Fig. 1 was drawn in Biorender (https://biorender.com/). Assimilation plots, PCA and HCA were created in JMP® version 15. All figures were finalized in Adobe Illustrator.

Acknowledgements

This research was funded by the Cystic Fibrosis Foundation (CFF), grant number MOLIN18G0, the Cystic Fibrosis Trust, Strategic Research Centre Award – 2019 – SRC 017, and the Novo Nordisk Foundation Center for Biosustainability, grant number NNF10CC1016517. H.K.J. was supported by The Novo Nordisk Foundation as a clinical research stipend (NNF12OC1015920), by Rigshospitalets Rammebevilling 2015–17 (R88-A3537), by Lundbeckfonden (R167-2013-15229), by Novo Nordisk Foundation (NNF15OC0017444), by RegionH Rammebevilling (R144-A5287), by Independent Research Fund Denmark/Medical and Health Sciences (FTP-4183-00051) and by 'Savværksejer Jeppe Juhl og Hustru Ovita Juhls mindelegat'. The financial support from The Novo Nordisk Foundation (grants NNF20CC0035580 and LiFe, NNF18OC0034818), the Danish Council for Independent Research (*SWEET*, DFF-Research Project 8021-00039B) and the European Union's Horizon 2020 Research and Innovation Programme under grant agreement No. 814418 (*SinFonia*) to P.I.N. is also gratefully acknowledged. We are grateful to Lars Boje Petersen and Mette Kristensen at the Analytics Core for their assistance with HPLC measurements, to Douglas McCloskey at the Computational Biology group and Daniel Christoph Volke and Systems Environmental Microbiology group for inputs on the implementation of the dilution-resolved method.

Conflicts of interest

The authors declare no competing or financial interests.

Data availability

The data that support the findings of this study are openly available in the Table S1.

References

Arce-Rodríguez, A., Nikel, P.I., Calles, B., Chavarría, M., Platero, R., Krell, T., and de Lorenzo, V. (2021) Low CyaA expression and anti-cooperative binding of cAMP to CRP frames the scope of the cognate regulon of *Pseudomonas putida*. *Environ Microbiol* **23:** 1732–1749.

Bartell, J.A., Sommer, L.M., Haagensen, J.A.J., Loch, A., Espinosa, R., Molin, S., and Johansen, H.K. (2019) Evolutionary highways to persistent bacterial infection. *Nat Commun* **10:** 629.

Behrends, V., Ebbels, T.M.D., Williams, H.D., and Bundy, J.G. (2009) Time-resolved metabolic footprinting for nonlinear modeling of bacterial substrate utilization. *Appl Environ Microbiol* **75:** 2453–2463.

Behrends, V., Geier, B., Williams, H.D., and Bundy, J.G. (2013) Direct assessment of metabolite utilization by *Pseudomonas aeruginosa* during growth on artificial sputum medium. *Appl Environ Microbiol* **79:** 2467–2470.

Behrends, V., Williams, H.D., and Bundy, J.G.. (2014) Metabolic footprinting: extracellular metabolomic analysis. In *Pseudomonas Methods and Protocols*. Filloux, A.. and Ramos, J.-L.. (eds). New York, NY: Springer, pp. 281–292.

del Castillo, T., Ramos, J.L., Rodríguez-Herva, J.J., Fuhrer, T., Sauer, U., and Duque, E. (2007) Convergent peripheral pathways catalyze initial glucose catabolism in *Pseudomonas putida*: genomic and flux analysis. *J Bacteriol* **189:** 5142–5152.

Chubukov, V., Gerosa, L., Kochanowski, K., and Sauer, U. (2014) Coordination of microbial metabolism. *Nat Rev Microbiol* **12:** 327–340.

Crone, S., Vives-Flórez, M., Kvich, L., Saunders, A.M., Malone, M., Nicolaisen, M.H., *et al*. (2020) The environmental occurrence of *Pseudomonas aeruginosa*. *Apmis* **128:** 220–231.

Davis, R., Duane, G., Kenny, S.T., Cerrone, F., Guzik, M.W., Babu, R.P., *et al*. (2015) High cell density cultivation of *Pseudomonas putida* KT2440 using glucose without the need for oxygen enriched air supply. *Biotechnol Bioeng* **112:** 725–733.

Deschamps, E., Schaumann, A., Schmitz-Afonso, I., Afonso, C., Dé, E., Loutelier-Bourhis, C., and Alexandre, S.

(2021) Membrane phospholipid composition of *Pseudomonas aeruginosa* grown in a cystic fibrosis mucus-mimicking medium. *Biochim Biophys Acta - Biomembr* **1863:** 183482.

Deutschbauer, A., Price, M.N., Wetmore, K.M., Tarjan, D.R., Xu, Z., Shao, W., *et al*. (2014) Towards an informative mutant phenotype for every bacterial gene. *J Bacteriol* **196(20):** 3643–3655.

van Ditmarsch, D., and Xavier, J.B. (2011) High-resolution time series of *Pseudomonas aeruginosa* gene expression and rhamnolipid secretion through growth curve synchronization. *BMC Microbiol* **11:** 140.

Dolan, S.K., Kohlstedt, M., Trigg, S., Vallejo Ramirez, P., Kaminski, C.F., Wittmann, C., and Welch, M. (2020) Contextual flexibility in *Pseudomonas aeruginosa* central carbon metabolism during growth in single carbon sources. *MBio* **11:** e02684-19.

Duetz, W.A. (2007) Microtiter plates as mini-bioreactors: miniaturization of fermentation methods. *Trends Microbiol* **15:** 469–475.

Duetz, W.A., and Witholt, B. (2004) Oxygen transfer by orbital shaking of square vessels and deepwell microtiter plates of various dimensions. *Biochem Eng J* **17:** 181–185.

Govantes, F. (2018) Serial dilution-based growth curves and growth curve synchronization for high-resolution time series of bacterial biofilm growth. In *Host-Pathogen Interactions: Methods and Protocols*. Medina, C., and López-Baena, F.J. (eds). New York, NY: Springer, pp. 159–169.

Hartmans, S., Smits, J.P., Van der Werf, M.J., Volkering, F., and De Bont, J.A.M. (1989) Metabolism of styrene oxide and 2-phenylethanol in the styrene-degrading Xanthobacter strain 124X. *Appl Environ Microbiol* **55:** 2850–2855.

Henriques, I.D.S., Aga, D.S., Mendes, P., O'Connor, S.K., and Love, N.G. (2007) Metabolic footprinting: a new approach to identify physiological changes in complex microbial communities upon exposure to toxic chemicals. *Environ Sci Technol* **41:** 3945–3951.

Howell, K.S., Cozzolino, D., Bartowsky, E.J., Fleet, G.H., and Henschke, P.A. (2006) Metabolic profiling as a tool for revealing Saccharomyces interactions during wine fermentation. *FEMS Yeast Res* **6:** 91–101.

Jiménez-Fernández, A., Lopez-Sanchez, A., Calero, P., and Govantes, F. (2015) The c-di-GMP phosphodiesterase BifA regulates biofilm development in *Pseudomonas putida*. *Environ Microbiol Rep* **7:** 78–84.

Jiménez-Fernández, A., López-Sánchez, A., Jiménez-Díaz, L., Navarrete, B., Calero, P., Platero, A.I., and Govantes, F. (2016) Complex Interplay between FleQ, cyclic diguanylate and multiple σ factors coordinately regulates flagellar motility and biofilm development in *Pseudomonas putida*. *PLoS One* **11:** e016314.

Kaderbhai, N.N., Broadhurst, D.I., Ellis, D.I., Goodacre, R., and Kell, D.B. (2003) Functional genomics via metabolic footprinting: monitoring metabolite secretion by *Escherichia coli* tryptophan metabolism mutants using FT-IR and direct injection electrospray mass spectrometry. *Comp Funct Genomics* **4:** 376–391.

Kragh, K.N., Alhede, M., Rybtke, M., Stavnsberg, C., Jensen, P.Ø., Tolker-Nielsen, T., *et al*. (2018) The inoculation method could impact the outcome of microbiological experiments. *Appl Environ Microbiol* **84:** 1–14.

La Rosa, R., Behrends, V., Williams, H.D., Bundy, J.G., and Rojo, F. (2016) Influence of the Crc regulator on the hierarchical use of carbon sources from a complete medium in *P. seudomonas*. *Environ Microbiol* **18:** 807–818.

La Rosa, R., Johansen, H.K., and Molin, S. (2018) Convergent Metabolic specialization through distinct evolutionary paths in *Pseudomonas aeruginosa*. *MBio* **9:** e00269-18.

La Rosa, R., Johansen, H.K., and Molin, S. (2019) Adapting to the airways: metabolic requirements of *Pseudomonas aeruginosa* during the Infection of cystic fibrosis patients. *Metabolites* **9:** 234.

López-Sánchez, A., Jiménez-Fernández, A., Calero, P., Gallego, L.D., and Govantes, F. (2013) New methods for the isolation and characterization of biofilm-persistent mutants in *Pseudomonas putida*. *Environ Microbiol Rep* **5:** 679–685.

López-Sánchez, A., Leal-Morales, A., Jiménez-Díaz, L., Platero, A.I., Bardallo-Pérez, J., Díaz-Romero, A., *et al*. (2016) Biofilm formation-defective mutants in *Pseudomonas putida*. *FEMS Microbiol Lett* **363:** fnw127

Mapelli, V., Olsson, L., and Nielsen, J. (2008) Metabolic footprinting in microbiology: methods and applications in functional genomics and biotechnology. *Trends Biotechnol* **26:** 490–497.

McGill, S.L., Yung, Y., Hunt, K.A., Henson, M.A., Hanley, L., and Carlson, R.P. (2021) *Pseudomonas aeruginosa* reverse diauxie is a multidimensional, optimized, resource utilization strategy. *Sci Rep* **11:** 1–16.

Molina, L., La Rosa, R., Nogales, J., and Rojo, F. (2019a) Influence of the Crc global regulator on substrate uptake rates and the distribution of metabolic fluxes in *Pseudomonas putida* KT2440 growing in a complete medium. *Environ Microbiol* **21:** 4446–4459.

Molina, L., La Rosa, R., Nogales, J., and Rojo, F. (2019b) *Pseudomonas putida* KT2440 metabolism undergoes sequential modifications during exponential growth in a complete medium as compounds are gradually consumed. *Environ Microbiol* **21:** 2375–2390.

Nikel, P.I., Chavarría, M., Fuhrer, T., Sauer, U., and de Lorenzo, V. (2015) *Pseudomonas putida* KT2440 strain metabolizes glucose through a cycle formed by enzymes of the Entner-Doudoroff, Embden-Meyerhof-Parnas, and Pentose Phosphate pathways. *J Biol Chem* **290:** 25920–25932.

Nikel, P.I., Fuhrer, T., Chavarría, M., Sánchez-Pascuala, A., Sauer, U., and de Lorenzo, V. (2021) Reconfiguration of metabolic fluxes in *Pseudomonas Putida* as a response to sub-lethal oxidative stress. *ISME J* **15:** 1751–1766.

Nikel, P.I., Martínez-García, E., and de Lorenzo, V. (2014) Biotechnological domestication of pseudomonads using synthetic biology. *Nat Rev Microbiol* **12:** 368–379.

O'Brien, E.J., Monk, J.M., and Palsson, B.O. (2015) Using genome-scale models to predict biological capabilities. *Cell* **161:** 971–987.

Paczia, N., Nilgen, A., Lehmann, T., Gätgens, J., Wiechert, W., and Noack, S. (2012) Extensive exometabolome analysis reveals extended overflow metabolism in various microorganisms. *Microb Cell Fact* **11:** 1–14.

Palmer, K.L., Aye, L.M., and Whiteley, M. (2007) Nutritional cues control *Pseudomonas aeruginosa* multicellular behavior in cystic fibrosis sputum. *J Bacteriol* **189:** 8079–8087.

Rojo, F. (2010) Carbon catabolite repression in Pseudomonas: optimizing metabolic versatility and interactions with the environment. *FEMS Microbiol Rev* **34:** 658–684.

Rossi, E., La Rosa, R., Bartell, J.A., Marvig, R.L., Haagensen, J.A.J., Sommer, L.M., *et al.* (2021) *Pseudomonas aeruginosa* adaptation and evolution in patients with cystic fibrosis. *Nat Rev Microbiol* **19:** 331–342.

Sezonov, G., Joseleau-Petit, D., and D'Ari, R. (2007) *Escherichia coli* physiology in Luria-Bertani broth. *J Bacteriol* **189:** 8746–8749.

Turner, K.H., Wessel, A.K., Palmer, G.C., Murray, J.L., and Whiteley, M. (2015) Essential genome of *Pseudomonas aeruginosa* in cystic fibrosis sputum. *Proc Natl Acad Sci USA* **112:** 4110–4115.

Weimer, A., Kohlstedt, M., Volke, D.C., Nikel, P.I., and Wittmann, C. (2020) Industrial biotechnology of *Pseudomonas putida*: advances and prospects. *Appl Microbiol Biotechnol* **104:** 7745–7766.

Wewetzer, S.J., Kunze, M., Ladner, T., Luchterhand, B., Roth, S., Rahmen, N., *et al.* (2015) Parallel use of shake flask and microtiter plate online measuring devices (RAMOS and BioLector) reduces the number of experiments in laboratory-scale stirred tank bioreactors. *J Biol Eng* **9.** https://doi.org/10.1186/s13036-015-0005-0

Yung, Y.P., McGill, S.L., Chen, H., Park, H., Carlson, R.P., and Hanley, L. (2019) Reverse diauxie phenotype in *Pseudomonas aeruginosa* biofilm revealed by exometabolomics and label-free proteomics. *NPJ Biofilms Microbiomes* **5:** 31.

Zampieri, M., Sekar, K., Zamboni, N., and Sauer, U. (2017) Frontiers of high-throughput metabolomics. *Curr Opin Chem Biol* **36:** 15–23.

Supporting information

Additional supporting information may be found online in the Supporting Information section at the end of the article.

Fig. S1. Assimilation plots of all quantified metabolites for *Pseudomonas aeruginosa* PAO1 cultivated in SCFM. The concentration of each metabolite in Erlenmeyer flasks (blue symbols and lines), and deep-well plates (red symbols and lines) is shown relative to the OD at which supernatant samples were collected. Shaded areas indicate the 95% confidence intervals of the curves (cubic spline fitting).

Fig. S2. Assimilation hierarchy (A and B) and assimilation rate (C and D) determined using the data from three (blue bars) or two (red bars) biological replicates for the dilution-resolved (A and C) and time-resolved (B and D) methods. The error bar indicates the SEM (Standard Error of the Mean). Differences between rates were evaluated by Unpaired Welch *t*-test with significance indicated as 'ns' where $P > 0.05$ and '**' where $P < 0.01$.

Table S1. Data tables of metabolomics data for *Pseudomonas putida* and *Pseudomonas aeruginosa*; hierarchy and rate of assimilation; SCFM composition.

